



On Human-like Biases in Convolutional Neural Networks for the Perception of Slant from Texture

YUANHAO WANG and QIAN ZHANG, Brown University Department of Computer Science, USA
CELINE AUBUCHON, JOVAN KEMP, and FULVIO DOMINI, Brown University Department of
Cognitive, Linguistic, and Psychological Sciences, USA
JAMES TOMPKIN, Brown University Department of Computer Science, USA

Depth estimation is fundamental to 3D perception, and humans are known to have biased estimates of depth. This study investigates whether convolutional neural networks (CNNs) can be biased when predicting the sign of curvature and depth of surfaces of textured surfaces under different viewing conditions (field of view) and surface parameters (slant and texture irregularity). This hypothesis is drawn from the idea that texture gradients described by local neighborhoods—a cue identified in human vision literature—are also representable within convolutional neural networks. To this end, we trained both unsupervised and supervised CNN models on the renderings of slanted surfaces with random Polka dot patterns and analyzed their internal latent representations. The results show that the unsupervised models have similar prediction biases as humans across all experiments, while supervised CNN models do not exhibit similar biases. The latent spaces of the unsupervised models can be linearly separated into axes representing field of view and optical slant. For supervised models, this ability varies substantially with model architecture and the kind of supervision (continuous slant vs. sign of slant). Even though this study says nothing of any shared mechanism, these findings suggest that unsupervised CNN models can share similar predictions to the human visual system. Code: github.com/brownvc/Slant-CNN-Biases

CCS Concepts: • **Computing methodologies** → *Shape inference*; Perception;

Additional Key Words and Phrases: Perception, slant, texture, convolutional neural networks, deep learning

ACM Reference format:

Yuanhao Wang, Qian Zhang, Celine Aubuchon, Jovan Kemp, Fulvio Domini, and James Tompkin. 2023. On Human-like Biases in Convolutional Neural Networks for the Perception of Slant from Texture. *ACM Trans. Appl. Percept.* 20, 4, Article 15 (October 2023), 18 pages.

<https://doi.org/10.1145/3613451>

YW, QZ, and JT thank NSF IIS-2107409 and CAREER-2144956. CA, JK, and FD thank NSF BCS-2120610 and NIH 1R21EY033182-01A1.

Authors' addresses: Y. Wang, Q. Zhang, and J. Tompkin, Brown University Department of Computer Science, USA; emails: yuanhao_wang@alumni.brown.edu, qian_zhang@brown.edu, james_tompkin@brown.edu; C. Aubuchon, J. Kemp, and F. Domini, Brown University Department of Cognitive, Linguistic, and Psychological Sciences, USA; emails: celine_aubuchon@alumni.brown.edu, jovan_kemp@brown.edu, fulvio_domini@brown.edu.

Permission to make digital or hard copies of all or part of this work for personal or classroom use is granted without fee provided that copies are not made or distributed for profit or commercial advantage and that copies bear this notice and the full citation on the first page. Copyrights for components of this work owned by others than the author(s) must be honored. Abstracting with credit is permitted. To copy otherwise, or republish, to post on servers or to redistribute to lists, requires prior specific permission and/or a fee. Request permissions from permissions@acm.org.

© 2023 Copyright held by the owner/author(s). Publication rights licensed to ACM.

1544-3558/2023/10-ART15 \$15.00

<https://doi.org/10.1145/3613451>

1 INTRODUCTION

Deep neural networks have achieved success in a wide range of applications, such as image and speech recognition, natural language processing, and game playing. Since deep neural networks were originally inspired by the structure and function of the human brain, comparing deep neural networks to the human cognitive system has been an area of interest for researchers in the field of artificial intelligence and cognitive science.

The human visual system is a complex network of biological structures with remarkable but imperfect capabilities. Some works have tried to evaluate **convolutional neural networks (CNN)** as explanatory models for human vision using simulated psychophysical studies. A recent study by Storrs et al. [2021] considered the ambiguity between the perception of glossiness and surface curvature, where low-gloss high-curvature surfaces look the same as high-gloss low-curvature surfaces. They found that unsupervised neural networks made similar predictions to the human visual system in gloss perception: unsupervised networks could reproduce specific patterns of success and failure in distinguishing high and low gloss images commonly made by humans. Supervised networks trained to predict high or low gloss did not share this property. Given this finding, it is reasonable to ask whether unsupervised networks can exhibit human-like biases in visual tasks other than gloss perception.

We try to answer this question in the context of depth perception, where it is well-documented in vision science that humans are prone to bias [Campagnoli et al. 2022; Domini and Caudek 2003; Johnston 1991; Langer and Siciliano 2015; Liu and Todd 2004; Todd et al. 2007; Watt et al. 2005]. Specifically, we consider the task of estimating the perceived slant of textured surfaces. We consider simple Polka dot textures. Even with no other depth cues like disparity or shading, human beings can estimate surface slant because the texture deforms under perspective. Deformation under perspective is a subclass of the more general effect of shape from texture, where texture gradients provide a source of 3D shape information. Texture gradients are defined as the systematic variations of textures across neighboring regions [Gibson 1950a, b], with previous study into computational modeling of local neighborhoods under affine deformations to determine shape from texture [Malik and Rosenholtz 1997].

The setting of estimating slant from texture lets us investigate three additional influencing factors: the **field of view (FOV)**, the sign of the surface curvature (concave or convex), and texture pattern regularity. Previous research by Todd et al. [2005] found evidence for four biases. First, the perceived sign of curvature of a surface became ambiguous when the FOV was small. Second, an increase in FOV produced a corresponding increase in the magnitude of the perceptual gain (i.e., the judged slant divided by the ground truth). Third, humans perceive more depth from convex surfaces than from concave surfaces. Finally, there is a greater perceptual gain when the surface texture pattern is more regular. Some of these perceptual biases could be explained using texture gradients. When FOV is small or when texture elements are small, patterns of systematic change may be harder to discern, potentially causing errors or biases in slant estimation.

As a subclass of **deep neural networks (DNNs)**, it has been found that CNNs are good at modeling textures [Geirhos et al. 2018; Islam et al. 2021]. Their properties also make them potentially suited for the task of shape from texture: kernels as local neighborhood operators and aggregation across the visual field through multiple convolutional layers and down/upsampling layers. But, while CNNs are translation equivariant and may apply to statistically homogeneous textures (if we avoid the aliasing effects of max-pooling [Zhang 2019]), they do not naturally allow affine or perspective deformations of local neighborhoods. Considering these factors, a compelling avenue for investigation involves applying CNNs to the task of slant estimation from texture.

To test whether CNNs share such human biases, we followed the stimuli settings in Todd et al. [2005]. We generated synthetic renderings depicting surfaces with concave or convex dihedral angles, varying physical slant, varying FOV, and random Polka dot textures. Then, we trained unsupervised generative models to reconstruct the stimuli to learn the statistical regularities in the training data. From analyzing the learned network latent spaces, our study reveals that unsupervised models make predictions with human-like biases. They exhibit a higher error in judging the sign of curvature when FOV is smaller, perceive greater slant when FOV is increased, perceive more slant in convex surfaces than concave surfaces, and perceived more slant when texture regularity

increases. These results are consistent with the human findings in Todd et al. [2005], and suggest a similarity in the predictions made between the unsupervised deep neural networks and the human visual system (to say nothing of the mechanisms for those predictions). Across four different neural network architectures, we find some variation but overall similar trends in bias.

For the evaluated CNNs supervised with the signed continuous-valued surface slant, we discovered no bias on test stimuli. When considering the latent space separation of curvature sign, physical slant angle, and FOV, we find more significant differences across architectures than in unsupervised models, with one architecture leading to good factor separation and another not. Further, we also train a set of models with weaker supervision only of the sign of the surface curvature—concave or convex. This mirrors the ‘binary’ high/low gloss choice in the work of Storrs et al. [2021]. With weaker supervision, models still do not exhibit bias on test stimuli, and model latent factors are less well separated for all architectures. This suggests that latent space visualizations must be interpreted carefully and not independently: Supervised models with appropriate architectures and labels can still factor physically-meaningful variables even if their predictions are unbiased, and training models on impoverished labels (continuous slant vs. sign of slant) may incorrectly imply the ability of an architecture to factor variation.

2 BACKGROUND

2.1 Human Perceptual Biases in Depth Estimation

Understanding the mechanism of human depth perception is essential in 3D vision research. Humans integrate many sources of information to estimate depth, including binocular disparity, texture, shading, defocus, and motion, ultimately forming a three-dimensional percept of an object. A body of research has emerged to study human perceptual biases in depth judgment, and these biases can be categorized based on their associated visual cues.

For disparity, despite retinal and extra-retinal cues often providing sufficient information to achieve veridical perception, the visual system still produces errors. Johnston [1991] showed that the veridicality of human perception depends on the distance, with objects appearing elongated at a close viewing distance and flattened at a far distance. Ambiguities also exist within focus/de-focus cues: the sign of depth is ambiguous [Watt et al. 2005], and increasing blur gradient away from fixation point increases perceived slant [Langer and Siciliano 2015]. Liu et al. [2004] reported that participants exhibited biases in shape from shading as they misperceived convex surfaces as deeper. In addition, adding more sources of information from shading (i.e., specular highlights and cast shadows) increased perceived depth for convex surfaces. When using motion as a cue, the perceived depth depends on the deformation component of the optic flow field. This information is ambiguous and can lead to biases in depth perception [Domini and Caudek 2003]. Although increasing the number of available cues can potentially disambiguate depth information and lead to veridical perception, it has been shown that adding cues increases perceived depth without necessarily making it more accurate [Campagnoli et al. 2022].

The cue that is important to our study is texture. Studies have found that the sign of surface curvature, the field of view, and texture regularity can lead to perceptual biases in judging slant from texture [Todd et al. 2005, 2007].

- (B1) **Sign of curvature:** Convex surfaces appear to elicit greater slant responses than concave surfaces from humans.
- (B2) **Field of View Effect:** Large fields of view produce greater amounts of perceived slant than small fields of view.
- (B3) **Field of View Error:** Humans are more prone to err in judging the sign of surface curvature with small FOV.
- (B4) **Texture regularity:** Humans tend to perceive more slant from regular textures or textures with discrete elements. Compressing elements along one direction also increases perceived slant.

2.2 Unsupervised Models May Predict Human Perception

Many of the key ideas in machine learning took inspiration from the biological findings in the human brain. Most notably, neural networks mimic the design of interconnected biological neurons that send electrical signals to each other in a brain, and the **convolutional neural network (CNN)** was inspired by the hierarchical structure of the ventral visual pathway. Naturally, evaluating **deep neural networks (DNN)** as a model of the visual system has been a research area of interest. Many studies have found that DNNs trained for object recognition are good at predicting the representations of images in high-level ventral visual areas of the human and nonhuman primate brain [Kubilius et al. 2019; Lindsay 2021; Ponce et al. 2019; Schrimpf et al. 2018; Xu and Vaziri-Pashkam 2021].

The work most relevant to our methodology is that of Storrs et al. [2021]. The authors investigated the connection between intermediate representations in unsupervised models and the patterns of ‘success’ and ‘failure’ in human perception of gloss. They trained a **variational auto-encoder (VAE)** on a synthetic dataset consisting of renderings of bumpy surfaces with either high or low specular reflectance and found disentanglement of distal scene properties in the model’s latent space. Then, they trained a linear support vector machine classifier to generate quantitative gloss predictions. Surprisingly, the authors found that the latent codes of the unsupervised generative model could be used to predict human bias of gloss perception better than supervised networks or other control models. In our work, we try to test if unsupervised generative networks could also predict human bias related to slant estimation as well.

3 METHOD

To test whether unsupervised models exhibit human-like perceptual biases for slant estimation from texture cues, we first rendered a dataset of stimuli images. Next, we trained unsupervised generative CNN models to learn the statistical distributions of the data, along with supervised equivalent models for comparison. Then, we analyze the internal latent representations of each model to (a) evaluate how stimuli are laid out within it, and to (b) assess whether simple distance measures from linear classifiers on the latent space can produce biased outcomes.

3.1 Synthetic Data

We produced an *in silico* analogy of the real-world human psychophysical experimental setup of Todd et al. [2005] (Figure 1(a)). For a human being or a CNN to successfully estimate the physical slant, they must be able to separate the effects of varying view angles and slants on the deformations of the textures as no other cues exist. Note that the surface slant (ρ in Figure 1(a)) is directly correlated with the relative depth of the scene. For consistency and clarity, we choose to use the term slant for the rest of the paper.

Todd et al. use synthetic stimuli rendered to a 2D display surface, where the synthetic scene contained concave or convex dihedral angles that were bilaterally symmetrical about the vertical axis; whether the surface is concave or convex is referred to as the sign of curvature. In Todd et al.’s experimental design, the stimuli were rendered at 1280×1024 using computer graphics with a virtual perspective camera positioned at the center front of the surface, with a camera distance adjusted for each FOV so that the entire width of the surface was captured. The stimuli were shown on a display of a fixed size (30 cm on a CRT for $\text{FOV} \leq 20^\circ$, and 121.9 cm projected for $\text{FOV} > 20^\circ$), and the human observers examining the stimuli on the display were positioned at a viewing distance determined to ensure a visual angle corresponding to the camera angle used during rendering. This ensured that no bias could arise from incorrect geometric projections.

We follow Todd et al.’s experimental design, but now our observer is a CNN. To create stimuli, we positioned the virtual perspective camera at the center front of the surface and adjusted the viewing distance for each FOV so that the entire width of the surface was captured. Our stimuli are all generated at 256×256 resolution. We input the stimuli directly to the neural network; we have no human observer. This is different from the case where the human observer is moved to a viewing distance where no incorrect geometric projection is induced by an FOV/size mismatch. One way to think about the effect of this difference is to consider that, for

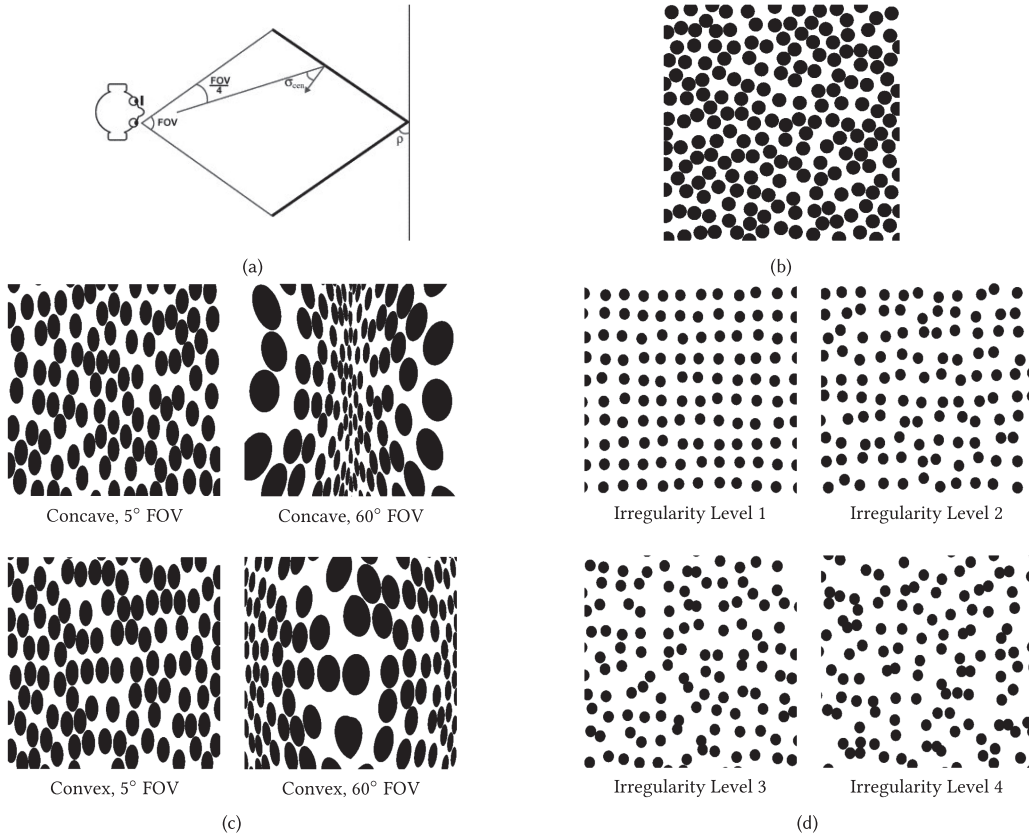


Fig. 1. Reproducing slant psychophysical experiments *in silico*. (a) A schematic top-view representation of the physical scene geometry used to depict the stimuli in the human psychophysical study (reproduced from Todd et al. [2005]), with surface slant ρ and optical slant σ_{cen} in the center of each face. (b) Random dot pattern projected onto a flat surface for reference. (c) Examples of our synthetic reproduction of the stimuli with a consistent optical slant of 60° and different dihedral angles and field of view (FOV). (d) Examples of textures with varying regularities rendered on a flat surface. Images have irregularity levels from 1 to 4.

the human, the perceived size of the stimuli still varies with observed distance. However, to the network and its convolutional kernels, the ‘observed size’ of the stimuli is fixed across FOVs. This induces an effective mismatched varying distance from which each slanted surface is seen [Todd et al. 2007]. We discuss this situation in Appendix A. Practically, a fixed-size stimuli gives a fixed-size unsupervised latent space, and lets us classify or regress outcomes in a supervised fashion using a **multi-layer perceptron (MLP)** head.

We generated stimuli with control over two parameters: the field of view (FOV) and the optical slant at the center of each surface (σ_{cen}). FOV ranged between 5° and 60° , and the values of σ_{cen} ranged between 25° and 60° . The ranges of optical slants for the concave and convex surfaces were matched (maximum value $\sigma_{max} = \sigma_{cen} + FOV/4$, minimum value $\sigma_{min} = \sigma_{cen} - FOV/4$). However, the physical slants (ρ), defined as $\rho = \sigma_{cen} + FOV/4$ for concave surfaces and $\rho = \sigma_{cen} - FOV/4$ for convex surfaces, had mismatched range.

For each combination of FOV, σ_{cen} , and curvature sign, we generated 10 random black and white Polka dot textures (Figure 1(b)). The dots were uniformly distributed with no overlaps and had the same size. We mapped each pattern onto the surface and rendered the scene using a perspective camera. The dataset consisted of 2,000 images, and all images were generated using Python. Figure 1(c) shows stimuli of different convexity and FOV.

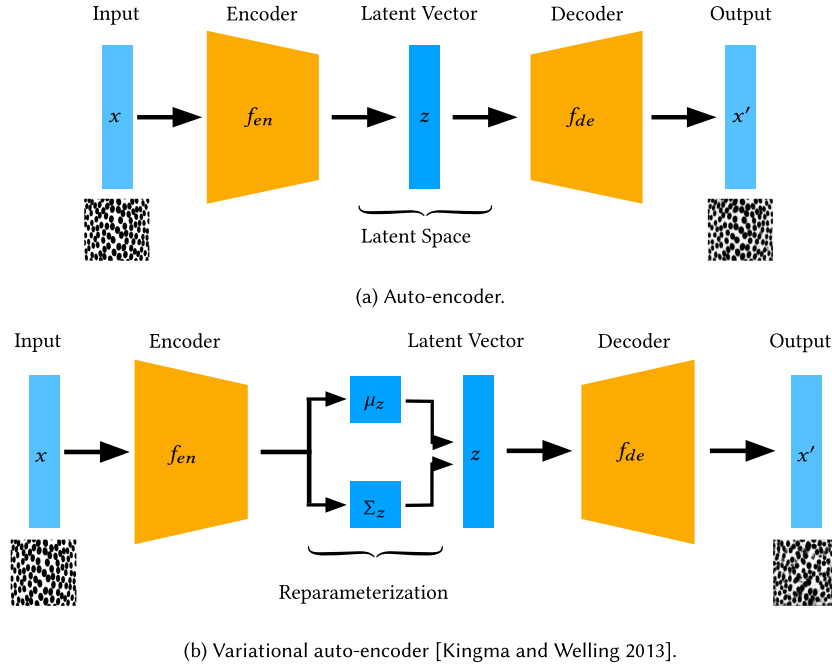


Fig. 2. Schematic illustration of neural network models.

To examine the impact of surface texture regularity on perceived slant from texture, we also generated stimuli with different Polka dot regularity (Figure 1(d)). The dot size was slightly smaller by 20% than previously to allow more dot variation to be visible at extremal slants. We began with a grid of uniform dots. Then, we shifted the center of each dot by α , where $\alpha \in R^2$, $\alpha \sim \mathcal{U}(-b, b)^2$. This allowed us to manipulate the regularity of the texture by adjusting b . In our experiments, we used five levels of variances/irregularities, ranging from level 0 (perfect grid) to level 4 (most irregular). As before, we mapped the surface dot patterns by the dihedral angles. We used FOV values in the range between 5° and 60° , and σ_{cen} values between 25° and 60° . This dataset comprised 10,000 images each of 256×256 pixels.

3.2 Unsupervised Generative Model

Unsupervised generative models are a class of neural networks trained to reproduce high-dimensional inputs. When trained on a large number of data points sampled from a distribution, their low-dimensional latent vectors are forced to encode the distribution as efficiently as possible. We trained generative models to reconstruct input 2D images. Our models are all auto-encoders (Figure 2(a)): an encoder compresses the input image to a low-dimensional latent space (often called a *bottleneck*), and a decoder restores the original input from the latent space. We evaluated several variants to investigate whether the study's findings were architecture-independent, with the primary architecture being the common U-Net [Ronneberger et al. 2015]. The model architectures are:

- (M1) **VGG-based auto-encoder (VGG-AE):** An auto-encoder that uses the VGG16 architecture [Simonyan and Zisserman 2014]. The encoder uses max pooling to downsample, and the decoder uses bilinear upsampling.
- (M2) **Variational auto-encoder (VAE):** We use the VAE proposed by Kingma et al. [2013]: Instead of passing the latent vector directly to the decoder, we add Gaussian noise to the latent vector with learned distribution parameters (Figure 2(b)). Storrs et al. [2021] used the PixelVAE variant to address blurry samples; the principle is the same.

- (M3) **U-Net** [Ronneberger et al. 2015]: This auto-encoder adds residual (or *skip*) connections between equivalent-spatial-sized layers of the encoder and the decoder networks. This lets high-resolution information pass directly from the encoder to the decoder, bypassing the bottleneck.
- (M4) **U-Net-**: This model removes the residual connections between the encoder and the decoder, so that all the information passed to the decoder is contained in the latent vector.

3.3 Supervised Model

To compare the behaviors of the unsupervised models to supervised ones, we conducted experiments with two different supervised architectures: a ResNet ([He et al. 2016]) model with 18 layers and a U-Net-based model that used the encoder of the U-Net. We augmented both architectures with an additional dense layer preceding the final layer, and treated its output space as the latent space similar to that of the unsupervised model. The models were trained using both stronger and weaker supervision: stronger physical slant labels and weaker sign of curvature labels. Collectively, these models let us examine the impact of different architectures and training objectives on the outcomes of the supervised models.

3.4 Network Details, Losses, and Training

All unsupervised and supervised models in our experiments have 64-dimensional latent spaces; network architectures are standard with our code available for further details. In terms of losses, the unsupervised objective is to reconstruct the input images. We penalize an L1 reconstruction loss, i.e., the sum of the absolute difference between each pair of matching pixels in the reconstructed and input images. Penalizing an L2 loss produced similar findings.

For supervised models, we have two settings. (1) We ask the network to predict the signed physical slant of the surface, as humans do in Todd et al. [2005]; and (2) We ask the network just to predict the sign of the physical slant of the surface; this mirrors the ‘binary’ high/low gloss choice in the work of Storrs et al. [2021].

Data are split into training and testing images with an 80/20% split. We train each model for 100 epochs using the Adam optimizer, with a learning rate of 2×10^{-4} , $\beta_1 = 0.5$, and $\beta_2 = 0.999$. As model training can show variability, we train an ensemble of 10 instances of each model and compute the mean and variance of their outputs; plots show standard error. After training, we fed unseen test images to the trained encoder to extract the latent vectors.

3.5 Methods of Analysis

Sign of curvature prediction. Unsupervised generative models cannot make predictions given a stimulus. However, it is possible to define a classifier upon the latent space. This assumes that a generative model can arrange stimuli in the latent space according to their statistical properties. For example, stimuli with the same sign of curvature may form clusters. Ideally, the physical properties form simple continuous arrangements. This would allow boundaries to be drawn using a linear classifier such as a **Support Vector Machine (SVM)**; it being linear allows only simple arrangements in the latent space to lead to meaningful interpretation. If stimuli are misplaced in the latent space, such as a concave stimulus being within convex stimuli, we can interpret this as an ‘error’ in judging convexity.

Magnitude of perceived slant. How far the latent code of a stimulus lies from the decision boundary can potentially be used as a measure of perceived slant. We compute the Euclidean distance of each latent code to the decision hyperplane, which we term the “latent distance”. We suppose that the latent distance is positively correlated with the magnitude of the perceived slant, and that stimuli with latent vectors lying on the decision boundary may be considered by the model as flat. A larger latent distance indicates that the model perceives the surface as more slanted, so that the model is more confident at predicting its sign of curvature. Although the

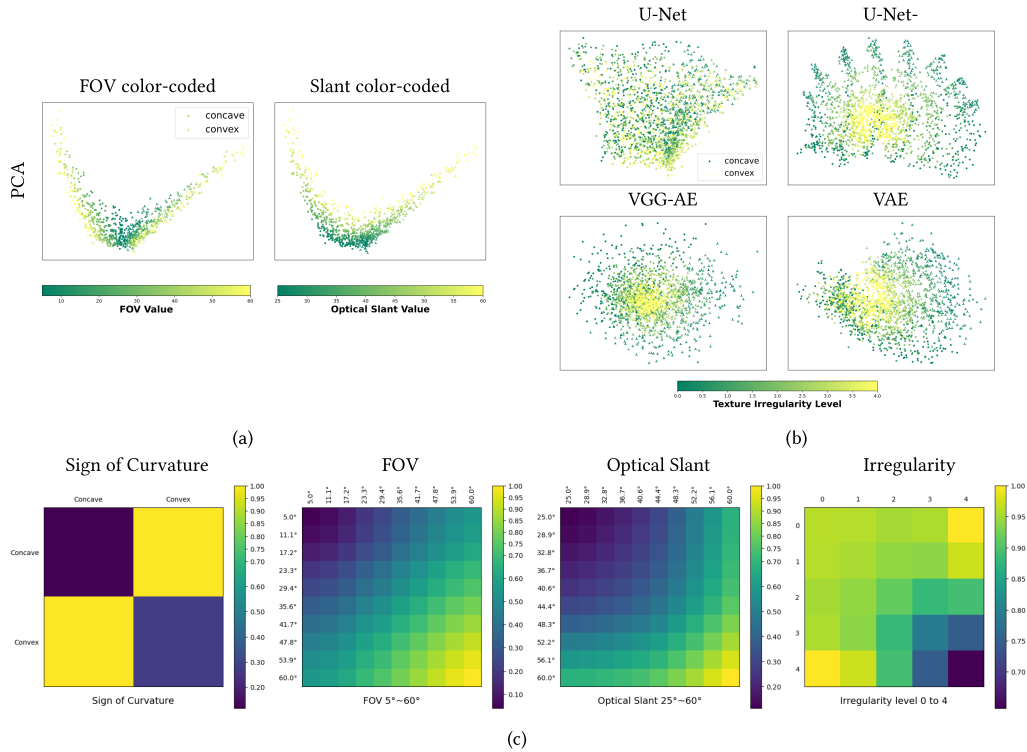


Fig. 3. Unsupervised model captures all physical factors in the latent space. (a) Unsupervised latent space visualizations. We visualize the latent space of the U-Net using PCA (first two principal components). Data points are color-coded by the FOV or the optical slant values. The unsupervised latent space disentangles surface convexity, FOV, and optical slant successfully. (b) Unsupervised latent space visualizations when trained on the dataset with varying texture irregularities. We visualize the latent spaces of all four unsupervised models, with data points color-coded by the texture irregularity level. All three alternative models disentangle texture irregularity levels, while the U-Net fails to do so. (c) Dissimilarity matrices showing mean distances between all pairs of latent vectors, grouped by the sign of curvature, FOV, optical slant values, and texture irregularity levels. Distances are defined as $1 - corr$, normalized to the range from 0 to 1, where $corr$ is the Pearson correlation coefficient. With the exception of U-Net with texture irregularity, the unsupervised models exhibit strong clustering by all factors; for texture irregularity, the U-Net- architecture instead shows strong clustering effects (shown here).

numerical value of the latent distance does not have physical meaning, we will use it to compare the perceived slants of different stimuli within the test set.

4 EXPERIMENTAL FINDINGS

4.1 Physical Factors are Disentangled in Unsupervised Model Latent Spaces

We are interested in the extent to which the unsupervised model can learn to disentangle our physical factors of interest in its latent representation—sign of curvature, field of view, optical slant, and texture regularity. First, we trained models on the dataset without texture irregularity discrepancies. After compressing the latent vectors to 2D using **principal component analysis (PCA)**, we observed grouping of concave and convex surfaces (Figure 3(a)). However, entanglement would occur if the latent dimension was too small (≤ 16 -dim.) or too large (≥ 256 -dim.). Furthermore, FOV and optical slant values varied smoothly within each cluster along two linearly separable axes, suggesting that both variables were well-disentangled in the latent space of the model.

Table 1. Correlations between FOV, Optical Slant, and the First Two Principal Components of the Latent Vectors

	Optical slant	FOV	FOV (concave)	FOV (convex)
1st P.C.	0.819	0.078	-0.190	0.239
2nd P.C.	0.480	0.252	0.551	-0.342

Next, we trained the unsupervised model on the dataset with varying levels of texture irregularities and visualized the latent spaces of all four models (Figure 3(b)). Notably, the U-Net model was unable to disentangle texture irregularity levels in its latent space. However, the same model could learn to disentangle texture irregularity if the residual connections between the encoder and the decoder were removed. In fact, all the tested unsupervised models without residual connections (U-Net-, VGG-AE, and VAE) exhibited discernible clusters based on the irregularity levels in the latent space. Images with less regular textures tended to concentrate in the middle region of the latent space, while images with more regular textures were more dispersed, indicating that the models were more capable of distinguishing input images with more regular textures.

We conducted a quantitative analysis on latent space clustering effects. Representational similarity analysis [Nili et al. 2014] showed that, for unsupervised models, pairs of images with the same convexity were represented by more similar vectors in the latent space than pairs of images with different convexity (Figure 3(c); T-test comparing average Euclidean distances between same-convexity versus different-convexity image pairs: $t = -200.20$; $P < 0.001$; Cohen’s $d = -0.71$; 95% **confidence interval (CI)** of difference, $-21.50 - -21.09$). Regarding FOV and optical slant, we observed that images with similar FOV or optical slant values tended to have similar latent representations; the dominant trend was that the latent representations became more spread out as FOV or optical slant increased (strong correlations between the FOV/optical slant and the averaged representational dissimilarity: $r = 0.979$ for FOV and $r = 0.956$ for optical slant). Moreover, the latent representations were more dissimilar when textures were more regular, which corroborated our prior observations from examining the latent spaces.

To quantify the ‘smoothness’ of latent space variations, we computed the strength of correlation between FOV, optical slant and the first two principal components of the latent vectors. There was strong correlation between the optical slant and the first principal component ($R = 0.819$), and moderately strong correlation between FOV and the second principal component when divided into concave and convex groups (Table 1; concave: $R = 0.551$, convex: $R = -0.342$). These results suggest that the unsupervised latent space smoothly captures FOV and optical slant variations.

4.2 Unsupervised Models Perceive More Slant with Greater FOV, Optical Slant, and Convex Surfaces

We use latent distance as a proxy for the magnitude of the perceived slant (Section 3.5). For the human bias that perceives more slant from convex surfaces than concave surfaces (**B1**), we observed that the unsupervised model exhibited a systematic bias towards perceiving more slant from convex surfaces than concave surfaces: The predicted latent distance in the convex cases was generally larger than that in the concave cases (Figure 4(d); cf. equivalent figure from Todd et al. [2005] reproduced beneath). Our qualitative observation is supported by the T-test results on the average difference in latent distance between the convex and concave groups, where the physical slant was between 26.25° and 58.75° ($t = 30.32$, $P < 0.001$). Further, experiments showed that the latent distance had a strong linear correlation with the FOV ($r = 0.998 \pm 0.001$; Figure 4(a) lower left), meaning the model perceived more slant as the FOV increased. Again, this is in line with the human perceptual bias (**B2**). Furthermore, the averaged latent distance was also positively correlated with the optical slant for each FOV value ($r = 0.980 \pm 0.002$; Figure 4(a) lower right).

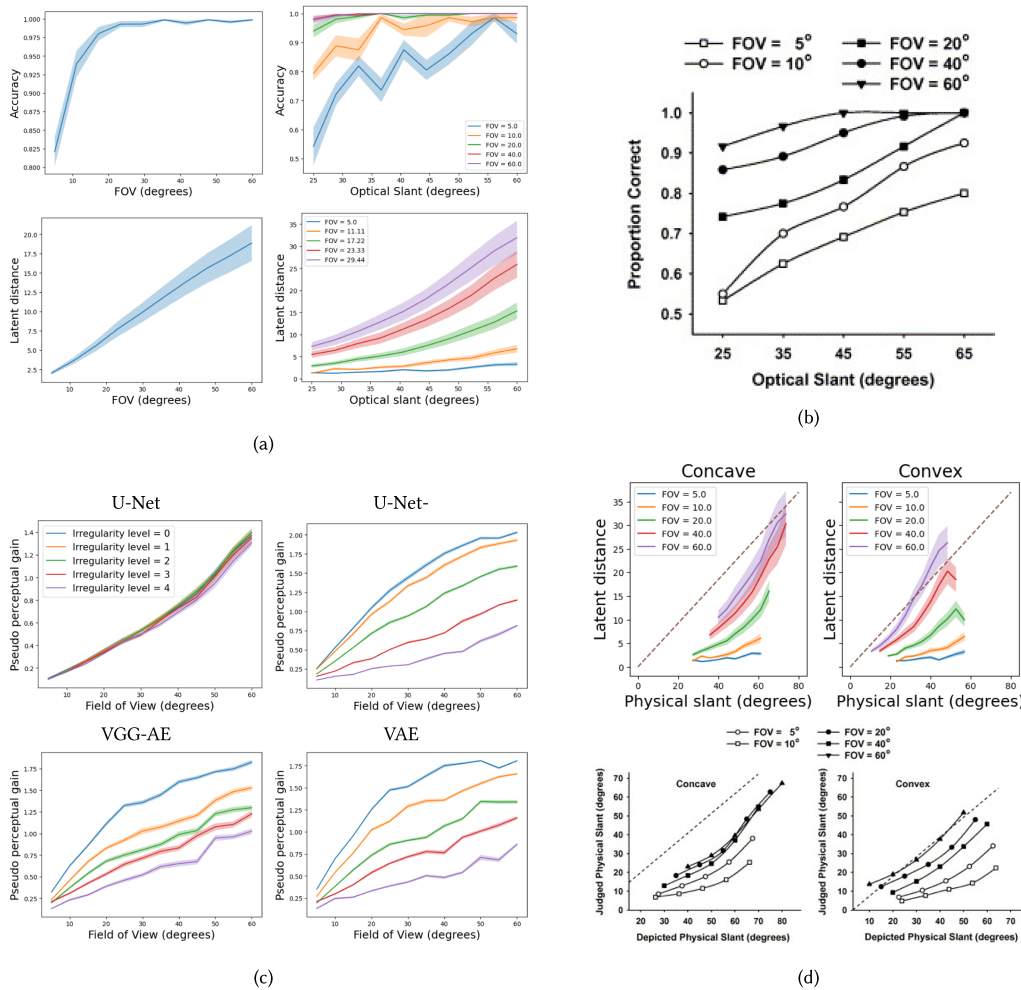


Fig. 4. Unsupervised models predict similar biases to humans in convexity and slant prediction. (a) Unsupervised model mean sign of curvature prediction accuracy and mean latent distance (rows) as functions of FOV and optical slant per FOV (columns). The mean prediction accuracy is 100% when the FOV is above 25° and increases with FOV and optical slant when the FOV is below 25°. The mean latent distance increases with both FOV and optical slant. (b) Results from human psychophysical study [Todd et al. 2005]. Humans accuracy in judging the sign of curvature also increases with both FOV and optical slant. (c) The pseudo perceptual gain as a function of the FOV per irregularity level for each tested model. With the exception of the U-Net that models texture detail primarily through residual connections, all other models produce greater pseudo perceptual gains with more regular textures. (d) Top row: unsupervised model’s latent distance as a function of the physical slant in concave and convex cases; bottom row: human psychophysical study results [Todd et al. 2005]. Both the unsupervised model and the human obtain larger perceptual gains from convex surfaces than from concave surfaces.

To better understand the effect of each variable, we computed generalized linear models [Nelder and Wedderburn 1972] separately on the set of concave and convex instances, using physical slant and FOV as independent variables and latent distance as the dependent variable. In both groups, physical slant and FOV are positively correlated with the latent distance with high pseudo R values (Table 2). Three-way **analysis of variance (ANOVA)**

Table 2. Generalized Linear Model Results for Unsupervised Case

Convexity	Variable	Coeff.	Std. err.	P-value	Pseudo R
Concave	P.S.	0.043	0.007	<0.010	0.844
	FOV	0.125	0.010	<0.001	
Convex	P.S.	0.056	0.005	<0.001	0.740
	FOV	0.075	0.005	<0.001	

The independent variables are physical slant (P.S.) and FOV, and the dependent variable is latent distance.

Table 3. Correlation Coefficients (R) between Texture Attributes and the Model’s Judged Slant (Latent Distance)

	Length	Width	Area	Spatial Density
Minimum value	0.852	0.353	0.609	0.658
Median value	0.911	0.739	0.843	0.657
Maximum value	0.924	0.852	0.835	0.644
Range	0.904	0.908	0.819	0.557

showed that FOV, convexity, and physical slant have statistically significant impacts on the latent distance (FOV: $F_{9,721} = 12.6, p < 0.001$; convexity: $F_{1,721} = 41.7, p < 0.001$; physical slant: $F_{6,721} = 39.0, p < 0.001$).

We conducted correlation analyses to identify common attributes of texture upon which model slant judgments could be based. As in classical works, we considered the length, width, area, and vertical density of the Polka dots. For each variable, we calculated the minimum, maximum, median, and range of values. Subsequently, we computed the correlation coefficients between each of the above-mentioned measures and the latent distance (Table 3). Results show strong correlations between the latent distance and multiple texture statistics, suggesting that the unsupervised model may use these attributes to represent the data.

4.3 The Sign of Curvature is Ambiguous when the Field of View is Small

The linear SVM lets us determine the judged sign of curvature for each test instance to calculate a classification accuracy. The overall accuracy of the unsupervised model is 96.4% ($\pm 0.91\%$). The model can predict the sign of curvature perfectly when the FOV is greater than 25° , but shows more errors when the FOV is smaller (Figure 4(a)). The accuracy also increases with the optical slant. We found moderately strong correlation between FOV and the mean classification accuracy ($r = 0.674 \pm 0.028$), and stronger correlation between the optical slant and the mean classification accuracy ($r = 0.813 \pm 0.027$). These findings are consistent with those from Todd et al. [2005] (B3; Figure 4(b)). Like humans, unsupervised models were more likely to misjudge the sign of curvature when the FOV was small. All supervised models were able to make classifications with 100% accuracy. Hence, no such bias could be inferred.

4.4 Unsupervised Latent Spaces Disentangle Texture Regularity

Todd et al. [2005] demonstrated that more regular textures led to a greater perceptual gain, defined as the human-judged slant divided by the ground truth slant (B4; Figure 4(d)). Does a similar effect of texture regularity on slant perception exist in our context? We trained both supervised and unsupervised models using a dataset consisting of synthetic renderings of Polka dot patterns with varying degrees of irregularities. Subsequently, we analyzed model responses to subsets of the dataset that corresponded to each level of irregularity.

In Section 4.1, we showed that unsupervised models that lack residual connections between the encoder and decoder were able to disentangle texture irregularity levels in the latent spaces. Further investigations revealed that these models also exhibit a perceptual bias. To facilitate the comparison, we define pseudo perceptual gain as the normalized latent distance divided by the normalized physical slant. The pseudo perceptual gain is greater at lower irregularity levels for U-Net-, VGG-AE and VAE, while no such disparity was observed in U-Net (Figure 4(c)). Without bypassing the latent bottleneck, unsupervised models produce greater perceptual gains from more regular textures. Despite differences in the experimental settings, the prediction patterns of humans and unsupervised models are related.

4.5 The Effects of Model Architecture

In the previous section, the experimental results differed significantly for models with or without residual connections. To evaluate the generalizability of our findings to a broader class of unsupervised models, we replicate the previous experiments using four architectures (Section 3.2).

We observed a significant variation in reconstruction quality across models. U-Net achieved good image quality, VGG-AE and VAE suffered from blurriness and artifacts, and U-Net- failed to reconstruct finer details (Figure 5(a)). The superior performance of the U-Net can be attributed to the residual connections that allowed direct passage of information to the decoder, allowing the bottleneck to ignore high-frequency information. Without residual connections, U-Net- lacked detailed stimuli reconstruction capabilities.

Despite differences in reconstruction, all models were capable of disentangling the sign of curvature in their latent spaces. The latent spaces of U-Net-, VGG-AE, and VAE models formed distinct clusters for concave and convex surfaces, albeit without the ‘V’ shape in the PCA plots observed in the case of the U-Net model (Figure 5(b)). Additionally, the three alternative models also learned to disentangle FOV and optical slant in their latent spaces. Comparable to the baseline U-Net model, images with lower FOV or optical slant values tended to be located closer to the classification boundary in the latent spaces. Subsequent analysis revealed that differences in same-convexity and cross-convexity representational similarity were statistically significant, but their clustering effects were weaker than those observed in the U-Net model (U-Net-: $t = -187.57$, $P < 0.001$, Cohen’s $d = -0.67$; VGG-AE: $t = -30.34$, $P < 0.001$, Cohen’s $d = -0.15$; VAE: $t = -80.81$, $P < 0.001$, Cohen’s $d = -0.29$).

Further analyses indicated that the alternative unsupervised models display comparable trends to the U-Net in predicting the sign of curvature and the perceived slants, despite underlying latent spaces being less well-structured. They all achieved high overall accuracy in surface convexity prediction: 84.0% ($\pm 1.2\%$) for U-Net-, 98.0% ($\pm 0.1\%$) for VGG-AE, and 94.7% ($\pm 0.2\%$) for VAE. Figure 5(c) shows that all three unsupervised models exhibit high accuracy when the field of view (FOV) is large, and relatively lower accuracy when the FOV is small. Additionally, the average latent distance increases linearly with FOV and optical slant in all models. Although the optical slant vs. latent distance curves are less smooth for the U-Net-, VGG-AE and VAE due to the worse behavior of their learned latent spaces, the general trends are still observable. Moreover, T-tests show that the alternative unsupervised models are systematically biased towards perceiving more slant from convex surfaces (U-Net-: $t = -30.46$, VGG-AE: $t = -35.5$, VAE: $t = -33.7$; $p < 0.001$ in all cases). In conclusion, all the perceptual biases observed in the U-Net hold true for the alternative models.

4.6 Supervised Models Produce Unbiased Outcomes, but Latent Behaviors Depend on Training Setting

Supervised models with the objective to predict the provided labels are unbiased when successfully trained. In our experiments, we found that when supervised with sign of curvature labels, our models were able to make class predictions with 100% accuracy. Additionally, when trained with ground truth physical slant labels, the predicted slants did not have a statistically significant mean difference from the ground truth slants ($p = 0.688$), nor was there a statistically significant mean difference in predicted slants between concave and convex images ($p = 0.394$).

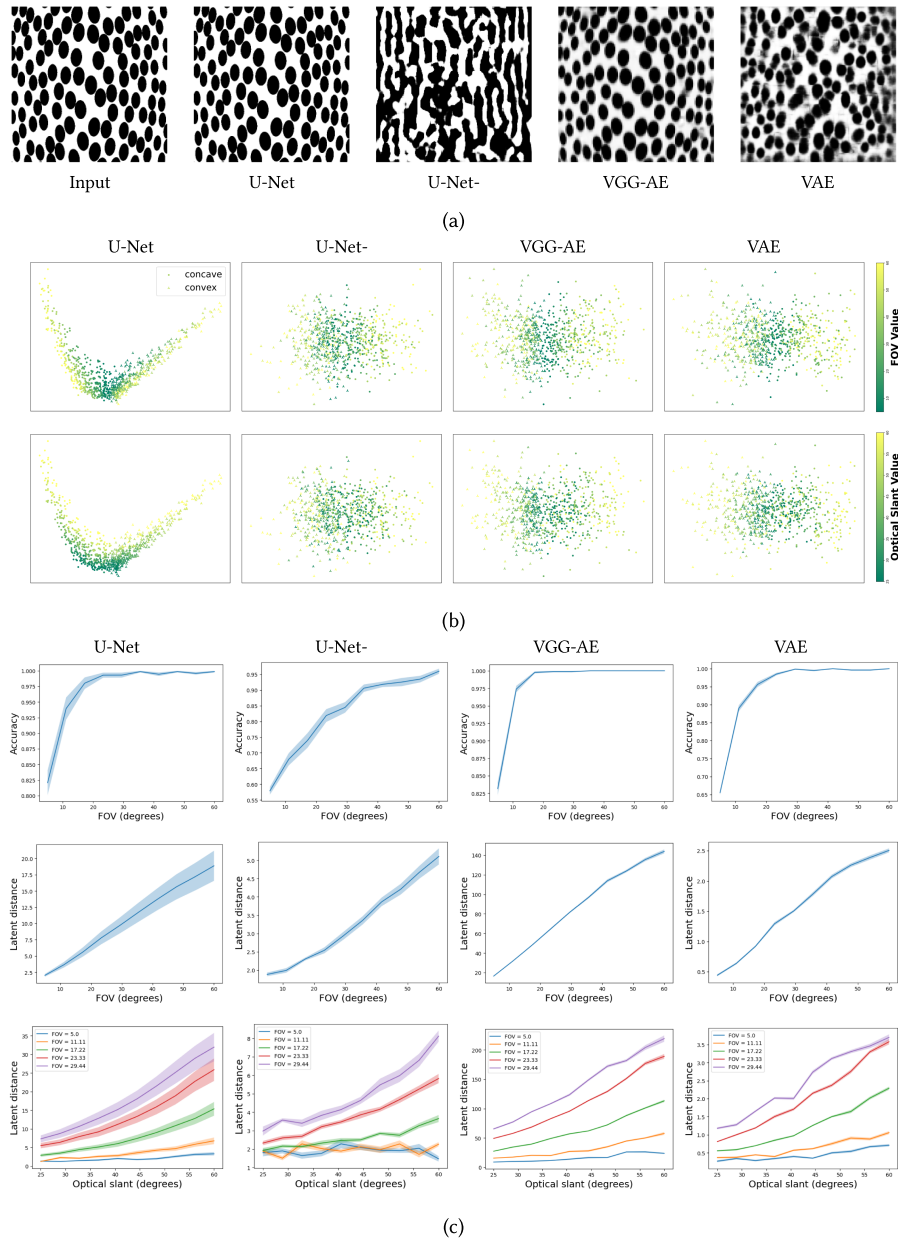


Fig. 5. Effects of unsupervised model architecture. (a) Reconstruction results of the unsupervised models show significant differences in quality across different models. (b) Latent space visualizations for the unsupervised models. Data points were color-coded by FOV and optical slant values (rows) for all four unsupervised models (columns). Sign of curvature, FOV and optical slant are disentangled by all models. (c) Latent space trend comparisons. Each row depicts a plot of a particular parameter against another, with the first row showing FOV vs. sign of curvature prediction accuracy, the second row showing FOV vs. latent distance, and the third row showing optical slant vs. latent distance per FOV. In each column, the plots are arranged from left to right to correspond to the models U-Net, U-Net-, VGG-AE, and VAE. The general trends are consistent across all models.

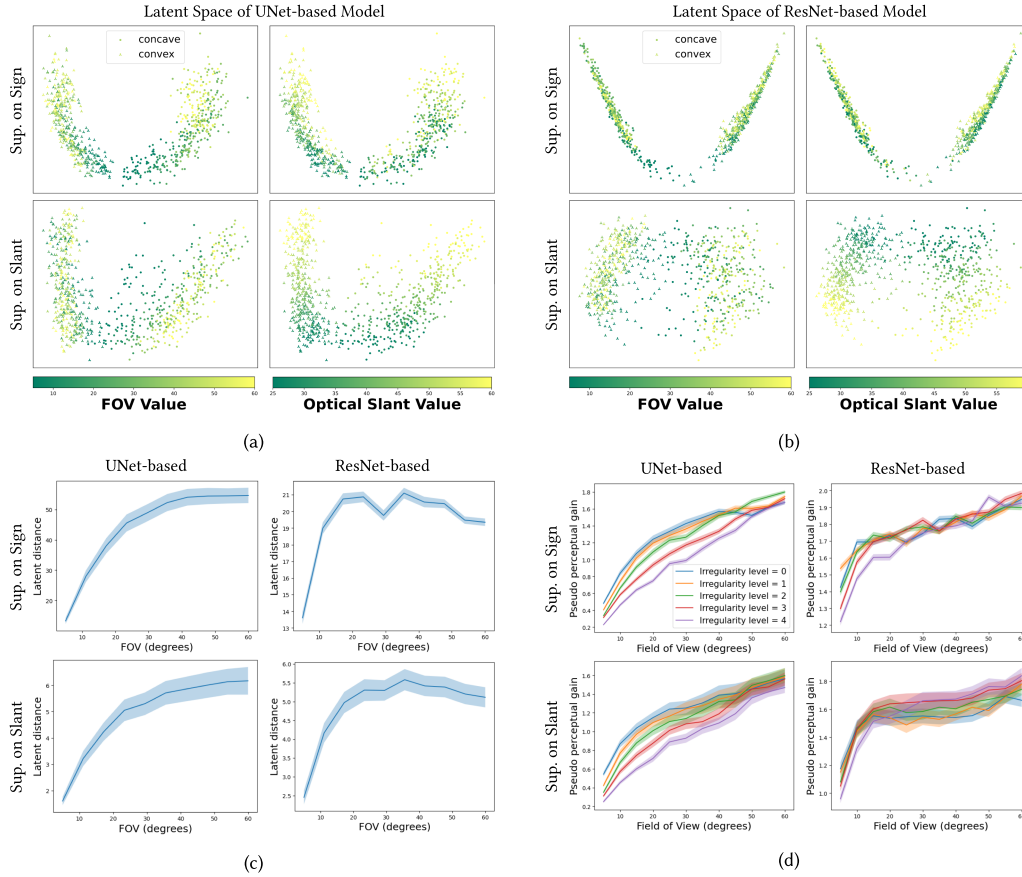


Fig. 6. Effects of supervised model architecture and training objective. (a) UNet-based supervised model latent space visualizations. We trained the model using the sign of curvature labels (top row) and physical slant values (bottom row). Data points are color-coded by the FOV and optical slant values (see legend). The latent space of the UNet-based supervised model captures FOV and slant regardless of the training objective, and the clustering effect is more substantial with stronger supervision (slant values). (b) For ResNet18 trained with curvature sign labels, there is a far separation of concave and convex stimuli in the latent space, but FOV and optical slant are entangled; trained with physical slant labels, optical slant is well disentangled and FOV is better separated. (c) Plots of the latent distance against the FOV for both training objective (rows) and model architectures (columns). U-Net-based supervised model has smoother curves, indicating a more structured latent space. (d) Pseudo perceptual gain as a function of the FOV per irregularity level for each supervised model (columns) and training objective (rows). Under both training settings, the supervised U-Net disentangles texture irregularity level and the ResNet fails to do so.

We examine the supervised latent spaces under different architectures and training settings. Figures 6(a) and 6(b) depict the latent space visualizations for the U-Net-based and ResNet-based models, respectively. They were trained using either sign of curvature labels or ground truth physical slant labels. Results indicate that both models, when supervised by the sign of curvature, exhibited a significant separation of concave and convex clusters in their respective latent spaces (U-Net: $t = -1036.07, P < 0.001$, Cohen's $d = -3.66$; ResNet: $t = -1461.17, P < 0.001$, Cohen's $d = -5.17$). However, in the ResNet-based model, the FOV and optical slant appeared to be fully entangled (FOV: $t = -18.07, P < 0.001$, Cohen's $d = -0.09$; Slant: $t = -4.27, P < 0.001$,

Cohen's $d = -0.02$), whereas the U-Net disentangled them (FOV: $t = -90.96, P < 0.001$, Cohen's $d = -0.46$; Slant: $t = -58.76, P < 0.001$, Cohen's $d = -0.29$).

On the other hand, model latent spaces were better structured when supervised by ground truth physical slant labels. This enabled both models to accurately cluster the optical slant (U-Net: $t = -258.48, P < 0.001$, Cohen's $d = -1.27$; ResNet: $t = -86.29, P < 0.001$, Cohen's $d = -0.43$), a variable directly related to physical slant, and to achieve better results at separating out FOV in the case of ResNet ($t = -40.77, P < 0.001$, Cohen's $d = -0.20$). The FOV vs. latent distance plots (Figure 6(c)) indicate that the latent distance first increases with FOV and then becomes flat in all cases, but the curves are smoother for the U-Net, indicating better latent space disentanglement. When trained on textures with different irregularities, the U-Net can disentangle texture irregularity under both training objectives, and the pseudo perceptual gain is greater at lower texture irregularity levels (Figure 6(d)). However, the ResNet fails at identifying texture irregularities in its latent space.

Across model architectures, supervised models showed stronger clustering with their supervised properties and weaker clustering with other properties, and their latent spaces better captured trained and untrained factors with stronger supervision.

5 DISCUSSION

How the human visual system learns to process and integrate visual depth cues to form a 3D percept remains unresolved in vision research. Notably, the human visual system exhibits various biases in depth perception, resulting in systematic deviations of the human predictions of depth from the ground truth under specific conditions.

Unsupervised DNNs can learn statistical distributions from high-dimensional inputs and compactly store information in latent representations. We have demonstrated that unsupervised CNNs are capable of predicting human-like biases in a range of tasks related to judging slant from texture. Specifically, unsupervised models perceived more slant when surfaces are convex rather than concave (**B1**; Section 4.2), perceived more slant when the FOV is greater (**B2**; Section 4.2), made more errors in determining the sign of surface curvature when the FOV is smaller (**B3**; Section 4.3), and perceived more slant when surface texture patterns are more regular (**B4**; Section 4.4). In comparison, no bias was observed when models were supervised by the ground truth.

While all factors of variation were well-disentangled in the unsupervised latent spaces, the choice of label and architecture was more important to the supervised CNNs. Factors of variation that were not trained upon were entangled: if trained on sign of curvature, then FOV and slant were entangled; if trained on slant, then FOV was entangled. As binary supervision, the impoverished sign of curvature provides less information to a network, and this significantly affected one architecture (ResNet) more than another (U-Net) due to the particular inductive biases of the architecture (e.g., coarse-to-fine encoder of U-Net). This demonstrates that careful interpretation is required when considering the efficacy of an architecture and training routine to factor variation within a latent space.

We found that modifying common design choices in CNN architectures (depth, width, convolution kernel size, activation functions, L1 vs. L2 loss) did not substantially affect the main conclusions of our study, despite impacting image reconstruction quality. One exception was the residual connections between the encoder and the decoder used in the U-Net. We empirically found that adding these additional paths that bypass the latent space bottleneck resulted in more structured latent spaces; such residual connections allow the latent space to ignore high-frequency spatial information that is hard to encode in layers with low spatial resolution. Despite preserving other perceptual biases, this modification impaired model ability to disentangle texture irregularity, perhaps because the model was less sensitive to high-frequency (small) irregularity changes. Further investigation is required to validate and explain this effect.

An overlooked aspect of this study pertains to the acuity of the networks. While we found that common design choices did not substantially affect the main conclusions, the size of the local neighborhood over which the network can reason does depend on the network's receptive field, and the texture gradient with respect to

a pixel does vary if images are rendered at different resolutions. To help reproduce varying fields of view to human observers, Todd et al. used stimuli at two fixed sizes (30 cm square on a CRT and 121.9 cm on a projector). Manipulating these two factors precisely may enable us to control model acuity and explore its effect on perceived latent slant.

Considering more complex textures, the psychophysical study by Todd et al. [2005] showed the impact of different texture types on human perception of depth—plaids, regular and irregular contours and blobs. Previous studies have also examined discrimination thresholds for human observers for slanted surfaces defined by more complex naturalistic textures such as Voronoi patterns, $1/f$ noise, and natural textures like leopard print. They found that humans were most precise for Polka dots and the least precise with noise patterns [Rosas et al. 2004]. Training a CNN autoencoder upon multiple distinct texture types is likely to create distinct latent space regions per texture type because the correlation in the data among textures may be larger than the correlation between textures across slants. One idea is to consider large datasets of complex natural textures, where broader trends such as slant may emerge in a latent space; works in learned generative models of texture may apply here [Yu et al. 2019].

Finally, we consider whether these results have implications for the study of 3D human perception. Todd et al. [2007] show that the patterns of biases discussed above can emerge if observers rely solely on image-level changes, such as measuring the scaling difference in the projected texture elements. Unsupervised shape from texture CNNs can provide a signal that is highly related to the shape of the surface, even though it does not produce the veridical estimate, and with an internal representation that is also highly correlated to geometric scaling measures of texture (Table 3). That said, neural networks find a good optimum under their training mechanism and data; when shown Polka dots under varying slant and FOV alone, it is natural to expect that the learned texture representation correlates to the input variation and that, when only image-level change exist and stimuli are hard to determine, similar prediction biases emerge in unsupervised settings. However, similar prediction does not imply a similar mechanism to achieve those predictions.

APPENDIX

A STIMULI AND EXPERIMENTAL LIMITATIONS

Section 3.1 details our attempt to closely follow the experimental setup of Todd et al. [2005] to generate stimuli for our experiments. However, a notable distinction existed between the real-world human psychophysical experiment and our *in silico* analogy in how to interpret ‘field of view’.

In the human experiment, observers were presented with a digital display showing computer graphics rendered stimuli seen at viewing distances such that the human’s visual field of view of the stimuli matched the graphics camera field of view used during rendering. This approach relies on the ability to move the viewer depending on the rendered FOV to remove any potential geometric distortion that would be induced by viewing the stimuli from an incorrect mismatched distance. However, varying viewing distances is difficult to achieve when passing stimuli into a CNN. This induces a mismatch that is conceptually similar to viewing stimuli of varying fields of view from a fixed distance.

Let us consider training a CNN in an unsupervised fashion on stimuli of a *fixed* field of view and at some pixel resolution, with physical slant as the varying property. The network’s kernels will model the distribution of texture variation under these slant changes. Now, let us render a test stimuli at the same pixel resolution but with a larger field of view. For any particular slant, the texture gradient induced by perspective distortion of the Polka dots must increase to fit more FOV into the same pixel resolution. Passing this stimuli into the CNN is akin to viewing the stimuli from a mismatched distance. Now, let us consider training a CNN on a general set of stimuli in which both field of view and slant vary (our experimental setting). Due to the fact that the pixel resolution does not change, this introduced a potential correlation in the data between FOV and the curvature induced by perspective distortion of the Polka dots, which is in principle identifiable by the network through its convolution kernels.

The impact of this correlation on the learned latent spaces remains uncertain and potentially problematic. A potential workaround could involve adjusting the resolutions of the input images based on their corresponding field of view values; yet, existing CNN architectures are not well suited to solving this problem because they are not easy to adapt to different image input sizes:

- (1) For a fixed set of network layers, varying stimuli size will produce varying sizes of intermediate latent spaces. In the unsupervised case, each different stimuli image size will produce a latent space of a different dimensionality, making later analysis difficult. The supervised case is similar: training an MLP to classify or regress requires a fixed-size intermediate latent space.
- (2) As the Polka dots are scaled for the stimuli to always contain a similar number regardless of the field of view, varying stimuli sizes will significantly vary the pixel size of the Polka dots. This requires kernels at large and significantly different sizes, adding computational cost, or a way for CNNs to better handle scale (e.g., through invariance or equivariance).

One alternative is to render all stimuli as inset partial images with respect to a maximal field of view. For example, at human-level acuity, a field of view of 60 degrees requires a stimuli of approximately $3,000 \times 3,000$ pixels, where smaller fields of view would only cover some of these pixels. This also adds significant computational cost, but at least alleviates the first problem above. Varying stimuli sizes requires there to be ‘empty space’ representing no content within each image. This could be black pixels; these must be masked within the loss and the contributions of the remaining pixels must be normalized for each stimuli. Initial experiments with this approach were not successful: The dominant variation captured by the model latent spaces is that of the stimuli size variation, not the underlying slant.

Solutions to these problems may exist, and future work should explore model architectures and training schemes that could enable the CNNs to perceive stimuli in a manner more analogous to human vision.

REFERENCES

- Carlo Campagnoli, Bethany Hung, and Fulvio Domini. 2022. Explicit and implicit depth-cue integration: Evidence of systematic biases with real objects. *Vision Research* 190 (2022), 107961.
- Fulvio Domini and Corrado Caudek. 2003. 3-D structure perceived from dynamic information: A new theory. *Trends in Cognitive Sciences* 7, 10 (2003), 444–449.
- Robert Geirhos, Patricia Rubisch, Claudio Michaelis, Matthias Bethge, Felix A. Wichmann, and Wieland Brendel. 2018. ImageNet-trained CNNs are biased towards texture; increasing shape bias improves accuracy and robustness. *arXiv preprint arXiv:1811.12231* (2018).
- James J. Gibson. 1950a. *The Perception of the Visual World*. (1950).
- James J. Gibson. 1950b. The perception of visual surfaces. *The American Journal of Psychology* 63, 3 (1950), 367–384.
- Kaiming He, Xiangyu Zhang, Shaoqing Ren, and Jian Sun. 2016. Deep residual learning for image recognition. In *Proceedings of the IEEE Conference on Computer Vision and Pattern Recognition*. 770–778.
- Md. Amirul Islam, Matthew Kowal, Patrick Esser, Sen Jia, Bjorn Ommer, Konstantinos G. Derpanis, and Neil Bruce. 2021. Shape or texture: Understanding discriminative features in CNNs. *arXiv preprint arXiv:2101.11604* (2021).
- Elizabeth B. Johnston. 1991. Systematic distortions of shape from stereopsis. *Vision Research* 31, 7-8 (1991), 1351–1360.
- Diederik P. Kingma and Max Welling. 2013. Auto-encoding variational Bayes. *arXiv preprint arXiv:1312.6114* (2013).
- Jonas Kubilius, Martin Schrimpf, Kohitij Kar, Rishi Rajalingham, Ha Hong, Najib Majaj, Elias Issa, Pouya Bashivan, Jonathan Prescott-Roy, Kailyn Schmidt, et al. 2019. Brain-like object recognition with high-performing shallow recurrent ANNs. *Advances in Neural Information Processing Systems* 32 (2019).
- Michael S. Langer and Ryan A. Siciliano. 2015. Are blur and disparity complementary cues to depth? *Vision Research* 107 (2015), 15–21.
- Grace W. Lindsay. 2021. Convolutional neural networks as a model of the visual system: Past, present, and future. *Journal of Cognitive Neuroscience* 33, 10 (Sep. 2021), 2017–2031. https://doi.org/10.1162/jocn_a_01544
- Baoxia Liu and James T. Todd. 2004. Perceptual biases in the interpretation of 3D shape from shading. *Vision Research* 44, 18 (2004), 2135–2145.
- Jitendra Malik and Ruth Rosenholtz. 1997. Computing local surface orientation and shape from texture for curved surfaces. *International Journal of Computer Vision* 2, 2 (1997), 149.
- John Ashworth Nelder and Robert W. M. Wedderburn. 1972. Generalized linear models. *Journal of the Royal Statistical Society: Series A (General)* 135, 3 (1972), 370–384.

- Hamed Nili, Cai Wingfield, Alexander Walther, Li Su, William Marslen-Wilson, and Nikolaus Kriegeskorte. 2014. A toolbox for representational similarity analysis. *PLoS Computational Biology* 10, 4 (2014), e1003553.
- Carlos R. Ponce, Will Xiao, Peter F. Schade, Till S. Hartmann, Gabriel Kreiman, and Margaret S. Livingstone. 2019. Evolving images for visual neurons using a deep generative network reveals coding principles and neuronal preferences. *Cell* 177, 4 (2019), 999–1009.
- Olaf Ronneberger, Philipp Fischer, and Thomas Brox. 2015. U-Net: Convolutional networks for biomedical image segmentation. In *Medical Image Computing and Computer-Assisted Intervention—MICCAI 2015: 18th International Conference, Munich, Germany, October 5–9, 2015, Proceedings, Part III* 18. Springer, 234–241.
- Pedro Rosas, Felix A. Wichmann, and Johan Wagemans. 2004. Some observations on the effects of slant and texture type on slant-from-texture. *Vision Research* 44, 13 (2004), 1511–1535. <https://doi.org/10.1016/j.visres.2004.01.013>
- Martin Schrimpf, Jonas Kubilius, Ha Hong, Najib J. Majaj, Rishi Rajalingham, Elias B. Issa, Kohitij Kar, Pouya Bashivan, Jonathan Prescott-Roy, Franziska Geiger, Kailyn Schmidt, Daniel L. K. Yamins, and James J. DiCarlo. 2018. Brain-score: Which artificial neural network for object recognition is most brain-like? *BioRxiv* (2018), 407007.
- Karen Simonyan and Andrew Zisserman. 2014. Very deep convolutional networks for large-scale image recognition. *arXiv preprint arXiv:1409.1556* (2014).
- Katherine R. Storrs, Barton L. Anderson, and Roland W. Fleming. 2021. Unsupervised learning predicts human perception and misperception of gloss. *Nature Human Behaviour* 5, 10 (2021), 1402–1417.
- James T. Todd, Lore Thaler, and Tjeerd M. H. Dijkstra. 2005. The effects of field of view on the perception of 3D slant from texture. *Vision Research* 45, 12 (2005), 1501–1517.
- James T. Todd, Lore Thaler, Tjeerd M. H. Dijkstra, Jan J. Koenderink, and Astrid M. L. Kappers. 2007. The effects of viewing angle, camera angle, and sign of surface curvature on the perception of three-dimensional shape from texture. *Journal of Vision* 7, 12 (2007), 9–9.
- Simon J. Watt, Kurt Akeley, Marc O. Ernst, and Martin S. Banks. 2005. Focus cues affect perceived depth. *Journal of Vision* 5, 10 (2005), 7–7.
- Yaoda Xu and Maryam Vaziri-Pashkam. 2021. Publisher correction: Limits to visual representational correspondence between convolutional neural networks and the human brain. *Nature Communications* 12 (2021).
- Ning Yu, Connelly Barnes, Eli Shechtman, Sohrab Amirghodsi, and Michal Lukac. 2019. Texture mixer: A network for controllable synthesis and interpolation of texture. In *Proceedings of the IEEE/CVF Conference on Computer Vision and Pattern Recognition*. 12164–12173.
- Richard Zhang. 2019. Making convolutional networks shift-invariant again. In *International Conference on Machine Learning*.

Received 6 July 2023; accepted 26 July 2023